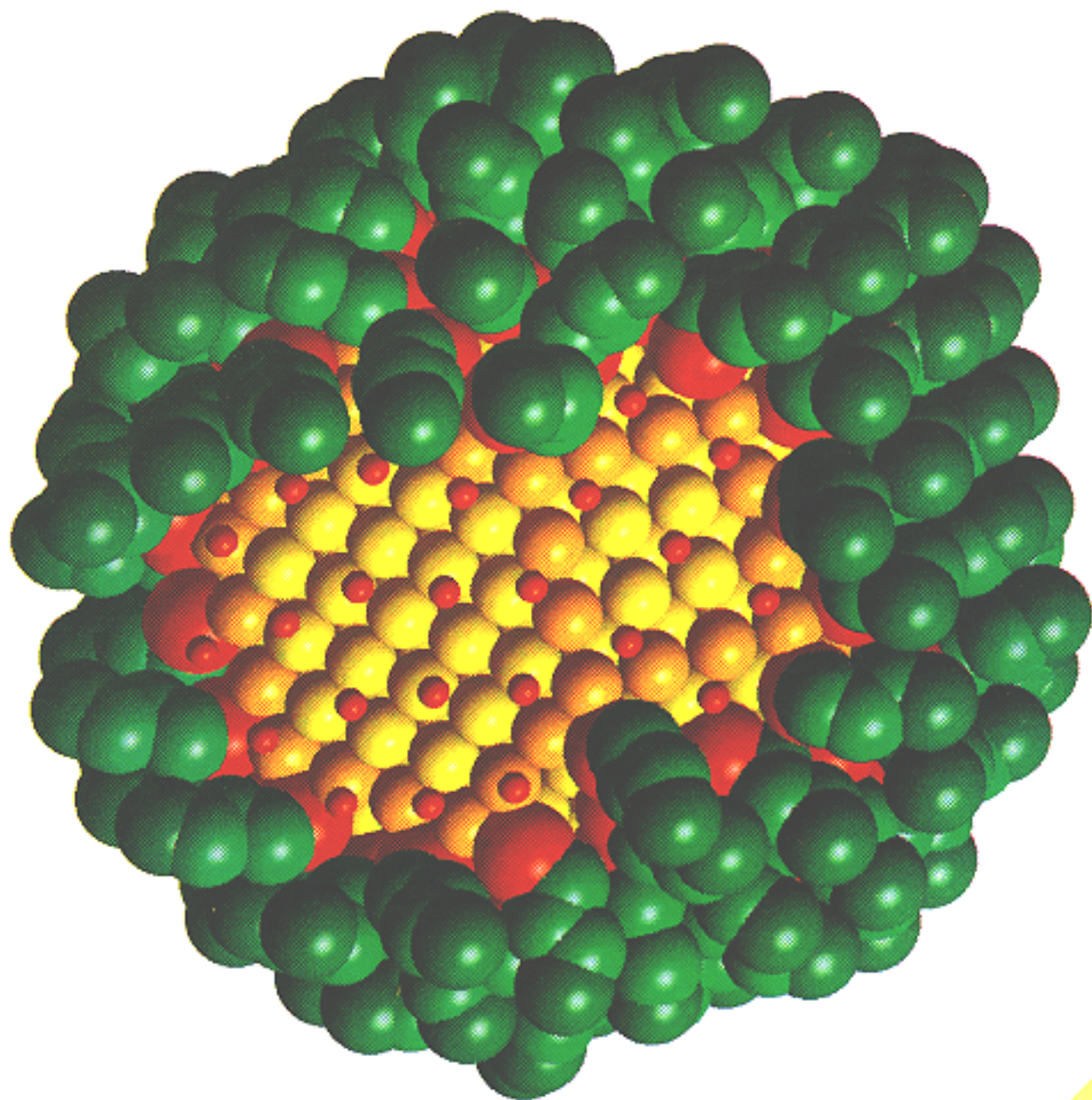


ADVMEW
ISSN 0935-9648
Vol. 8 - No. 5 - May 1996



ADVANCED MATERIALS



Passivated Nanocrystal Assemblies

Cascaded NLO Effects

Luminescent Conjugated Polymers

**CVD
section**

Nanocrystal Gold Molecules* *

By Robert L. Whetten,* Joseph T. Khoury, Marcos M. Alvarez, Srihari Murthy, Igor Vezmar, Z. L. Wang, Peter W. Stephens, Charles L. Cleveland, W. D. Luedtke, and Uzi Landman

The creation of perfect nanometer-scale crystallites (nanocrystals), identically replicated in unlimited quantities, in a state that can be manipulated and understood as pure macromolecular substances, is an ultimate challenge of modern materials research with outstanding fundamental and potential technological consequences.^[1] We report on the prediction, isolation, and characterization of a series of gold nanocrystals, passivated by self-assembled monolayers (SAMs) of straight-chain alkylthiolate molecules (RS, $R = n\text{-C}_n\text{H}_{2n+1}$),^[2] as highly purified molecular materials of high intrinsic stability. Such isolation is imperative for gaining a fundamental understanding of the nature of such materials and of the size-evolutionary patterns of their properties.

Analyses of members of this series of nanocrystals show that they belong to an energetically optimal sequence of structures, characterized by face-centered cubic (fcc) gold lattices and morphologies of a dominant truncated-octahedral motif. While each member of this series has a sharply defined mass, structure, and other properties characteristic of highly quantized lattices, electronic level structures, and band fillings, they also share common

features, including a propensity to form nanocrystal superlattices, and remarkable materials properties conferred by a strongly bound and compact protective layer.

Gold nanocrystals have been prepared by two entirely independent methods optimized to enhance the exclusive collection of very stable, passivated forms. In the first method, passivation of preformed metal nanocrystallites in the vapor phase is achieved by a technique described in detail elsewhere.^[3] The results shown below are on materials prepared by a second, solution-phase route,^[4] in which metal particles grow from metal ions reduced at the oil-water interface in the presence of an alkylthiolate surfactant (here $R = n\text{-C}_n\text{H}_{2n+1}$, except where stated otherwise) and a reducing agent.

The preparation is modified from that described earlier^[4] mainly by increasing the excess of the surfactant (1:2 Au:RS mole ratio), in order to enhance the surface saturation and stabilization of smaller nanocrystals, and by an extended exposure to a greater excess of the reducing agent in order to ensure adequate etching^[5] of defective structures initially formed. From either method, self-selected structures emerge that are stable against transformations, including growth or dissolution, amounting to a quantitative conversion of elemental gold into a macromolecular substance, which is stable under normal conditions in all forms (solutions, films, dry powders), completely redispersable in non-polar solvents, and exhibiting properties fully consistent with those expected to result from ideal passivation of the surface.

Initial examination of crude mixtures by high-resolution electron microscopy (HREM) shows that the particles each have compact, faceted, crystalline gold cores with diameters in the 1.5-3.5 nm range (and thus contain some 100 to 1300 Au atoms). At lattice-imaging resolution, only one in several hundred particles is found to be a multiply twinned gold crystallite (icosahedral or decahedral). Electron diffraction (ED) and powder X-ray diffraction (XRD) results indicate that the gold nanocrystals have fcc lattices with a mean lattice constant within 2 % of the bulk value ($a = 0.409$ nm). A mass spectrum (MS) of the crude mixture of passivated nanocrystals is shown in Figure 1 a, exhibiting a sequence of maxima in the 20 to 150 k region ($k = 10^3$ amu), in agreement with the HREM range. This pattern of abundance maxima is shown below to correlate with a predicted structural motif, and already suggests that passivated gold nanocrystals, prepared in this way, may exist predominantly in a distinct sequence of self-selected forms, which differ from each other sufficiently so that they can be separated quantitatively.

However, the separation and analysis of nanocrystal materials are generally rather formidable challenges,^[6] and in particular such materials had not previously been amenable to mass-spectrometric analysis. Therefore, it is significant that fractionation of the crude mixture has been accomplished, through cycles of fractional crystallization from solution, monitored at each stage by mass spectrometric analysis, repeated until each isolated component is amenable to structural analysis.

[*] Prof. R. L. Whetten, J. T. Khoury, Dr. M. M. Alvarez, Dr. S. Murthy, I. Vezmar

Schools of Physics and Chemistry, and
Microelectronics Research Center
Georgia Institute of Technology
Atlanta, Georgia 30332-043 (USA)

Dr. C. L. Cleveland, Dr. W. D. Luedtke, Prof. U. Landman
School of Physics, and

Center for Computational Materials Science
Georgia Institute of Technology
Atlanta, Georgia 30332-043 (USA)

Prof. Z. L. Wang
Schools of Materials Science and Engineering
Georgia Institute of Technology
Atlanta, Georgia 30332-043 (USA)

Prof. P. W. Stephens
Department of Physics
State University of New York
Stony Brook, NY 11794 (USA)

[**] The authors thank A. Wilkinson for discussion of early X-ray measurements; W. B. Carter for permission to mention photoelectron spectroscopic results; M. Duncan, J. Amster, T. P. Martin, and S. Frank for assistance in confirming and extending the mass spectrometry results; M. Shafiqullin for help in analyzing structural models; L. Saldana for performing spectroscopic and stability measurements; R. Whyman for stimulating discussions; and R. Andres for communication of results prior to publication. Financial support has been provided by the Georgia Tech Research Foundation, the Packard Foundation and the Office of Naval Research (to RLW), and the U.S. Department of Energy, the National Science Foundation, and the Air Force Office of Scientific Research (to CC, WDL, and UL). Calculations were performed on CRAY computers at the National Energy Research Supercomputer Center, Livermore, California, and at the GIT Center for Computational Materials Science.

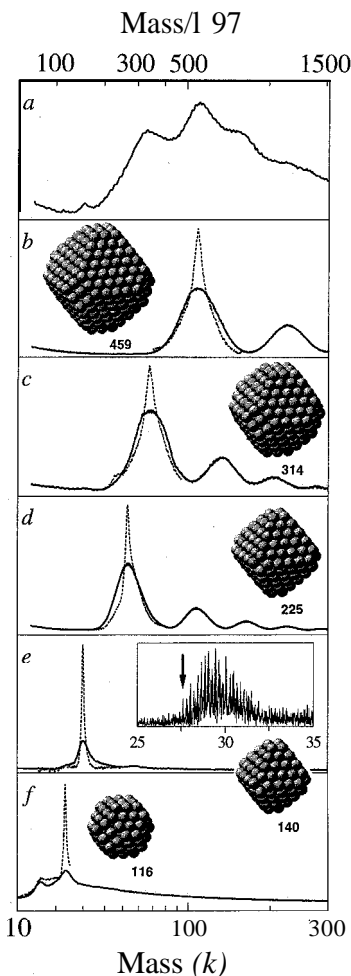


Fig. 1. Mass spectra (abundance vs. mass, in $k = 10^3$ amu, and in mass-equivalent number N of gold atoms, $m_{Au} = 197$ amu) for a crude mixture (a) and of separated fractions (b-e, corresponding to fractions I-IV, and f, a mixture of the two lightest fractions) of gold nanocrystals passivated by dodecane-thiolate monolayers. The inset structures are predicted optimal core structures containing $N = 459, 314$, etc. gold atoms (see text). Spectra are plotted versus cube-root of mass (or $N^{1/3}$) to facilitate comparison with measures of linear dimension. The inset to frame (e) is a high-resolution mass spectrum plotted on a linear mass scale, with an arrow marking the first peak at 27609 ± 2 amu.

A series of mass spectra for the dominant separated fractions is shown in Figure 1, confirming quantitative separation and yielding for each fraction an estimate for the number of Au atoms, N , in the gold nanocrystals (Table 1). The quality of separation is indicated by the absence of features on the base line leading up to the main peak in each spectrum (b-e); poorly separated fractions show steps or peaks in that region. The secondary peaks arise from aggregation occurring in the mass spectrometer; measurements on matrix-diluted samples (not shown) show a strong reduction of such features. In the conventional (lower-resolution) spectra (solid lines), the widths of the peaks arise from an undetermined influence of instrumental factors and mass dispersion resulting, for example, from a variable desorption of the surfactant monolayer.

Enhanced-resolution spectra (dotted lines in b-e) exhibit a significant narrowing of the main peaks, resulting in the upper bounds on the mass (and 'diameter') uncertainties listed in Table 1. The masses assigned in Table 1 for each fraction are taken from the inflection point in the rising portion of the main peak. Finally, the high-resolution spectrum (inset to Fig. 1e) shows a clear first peak at 27609 ± 2 amu, allowing one to establish the core mass and likely identity, $Au_{140}S$, for fraction IV. It is not clear whether

Table 1. Major fractions of nanocrystal gold molecules, enumerated (Roman numerals) in order of descending mass. The measured masses (and rms spreads thereof) are given both in units of $k = 10^3$ amu and of the number (N) of gold atoms (197 amu), along with distances (D_{111}^{MS} and D_{100}^{MS}) across the gold core in the [111] and [100] directions (Fig. 1), calculated from MS results assuming a regular truncated octahedron morphology and a gold number density of 59 nm^{-3} . The third column gives assignments to theoretically predicted N -atom fcc Au_N crystallites of the TO^- structural motif (see text and Fig. 1), their (n,m) indices, and their corresponding D_{111} and D_{100} distances. The intercrystallite center-to-center distances, $D_{XRD} = d_{111}$, are calculated from the small-angle (superlattice) X-ray diffraction peaks using the Bragg formula, $2d_{hkl} \sin \theta = \lambda$, with a bcc lattice indexing. The upper bound uncertainty in D_{XRD} is calculated from the full-widths at half-maximum of the first diffraction peak. A result obtained on a purified sample, prepared from an alternative solution phase method [20], is denoted by the symbol a. The TEM estimates of the mean particle diameters (D_{TEM}) and corresponding uncertainties are described in the text. All distances and lengths are given in nm.

	Mass (k) (N)	D_{111}^{MS} , D_{100}^{MS}	N (n,m)	D_{111} , D_{100}	D_{XRD}	D_{TEM}
I	93 ± 8 (472)	2.18, 2.52 $\pm 0.06, \pm 0.07$	4 5 9 (5,3)	2.1, 2.7 4.	1.1 f 0.0 9	2.4 ± 0.3
II	57 ± 7 (289)	1.85, 2.14 $\pm 0.08, \pm 0.08$	3 1 4 (4,3)	1.9, 2.3 3.9	3 f 0.0 7	2.0 ± 0.2
III	46 ± 3 (234)	1.73, 1.99 $\pm 0.04, \pm 0.04$	2 2 5 (5,2)	1.6, 2.3	3.52 ± 0.02	1.8 ± 0.3
N	27 ± 0.5 (137)	1.44, 1.67 $\pm 0.01, \pm 0.01$	1 4 0 (4,2)	1.4, 1.85 3	07" ± 0.05	NA

the sulfur atom has been captured from the dense, hot laser-desorption vapor, or remains from the thiol surfactant layer, nor has the increasingly complex structure in the 28 000–30 000 amu range a simple interpretation.

The occurrence and relative abundances of these stable passivated nanocrystals can be elucidated from predictions of the most stable forms of surfactant-free gold nanocrystals^[7] and from simulations of the packing structure of SAMs on these structures.^[8] Through an extensive search involving energy minimization^[7] employing realistic many-body embedded-atom potentials,^[9] the optimal structures for Au_N , $N > 40$, have been determined^[7b] to consist of finite fcc lattices with a polyhedral morphology of the truncated octahedral (TO) motif. Five of these predicted optimal fcc relaxed structures are shown in Figure 1, oriented with a [100] axis upright. Small centripetal displacements from the ideal (bulk) lattice positions occur primarily in the surface atomic layer near edges and vertices, resulting in a slight rounding of the overall crystallite shapes.

Characterization of these optimal structures may be given in terms of (n,m) indices, where n is the number of atoms on an edge adjoining (111) facets, and m that between adjoining (111) and (100) ones, including vertex atoms. Exposing (110) facets was explored and found to be energetically very unfavorable. In this description, for a regular TO polyhedron $n-m = 0$ ($n, m > 1$), while certain of its irregular variants are described as TO^- ($-4 \leq n-m < 0$, $m > 1$) and TO^+ ($0 < n-m \leq 4$, $m > 1$). Consideration of less-symmetric structures (obtained from the above by stepwise etching of individual facets) shows that energetically they belong to the same structural sequence, with no intermixing between structural motifs. Furthermore, we find that the faceted nature of the nanocrystals and their TO structural motif are maintained in simulations of gold nanocrystals with a compact monolayer of alkylthiolate molecules.^[8]

Of the theoretically analyzed structures in the $N=50$ to 500 range, a special subset of four (or five) clusters from the TO+ family emerges as having the greatest relative stability. This set comprises Au_{79} , Au_{140} , (Au_{225}), Au_{314} , Au_{459} , which as surfactant-free clusters would have masses near 16 k, 28 k, (45 k), 63 k, and 92 k. This pattern adequately accounts for the abundance maxima in the mass spectrum of the crude mixture (Fig. 1a). Motivated by these predictions, which are further corroborated below by direct structural information, we draw a correlation in Table 1 between the species in the separated fractions and the sequence of energetically favorable structures. The consistency of the structural and size assignments attained by this correlation, and the failure of other structural motifs, or combinations thereof, to account systematically for the observed pattern suggests that this assignment provides a sound framework for characterization and analysis of the materials.

Direct evidence for the fcc lattice structure and TO-faceted morphology of the gold cores of the passivated nanocrystals has been obtained from extensive HREM measurements on highly purified fractions, examples of which are shown in Figure 2. Figure 2a shows a selected image of a particle from fraction I, and the theoretically predicted plane-projected image of the $\text{TO}^+\text{Au}_{459}$ structure assigned to that fraction. The well-faceted gold core has its [110] axis oriented parallel to the electron beam (see inset for this image's 2D Fourier transform establishing this orientation), so that atomic columns appear as dark spots. This mono-crystalline structure, which measures 2.7 nm from top to bottom (parallel to a [100] direction) or

2.1 nm (parallel to [111]) is consistent with the 2D projection, along the same axis, of the theoretically energy-minimized structure, $\text{TO}^+\text{Au}_{459}$ (Fig. 1b), shown on the same scale at right.

HREM images also confirm the very narrow size-distribution and structural regularity in the individual fractions. In Figure 2b, the regularity in nanocrystal dimensions (size and shape) of fraction II, assigned to $\text{TO}^+\text{Au}_{314}$, is evident. Careful inspection of lattice fringe patterns establishes the particles as overwhelmingly mono-crystalline and well-faceted. A histogram of gold core dimensions obtained from this micrograph gives a size-distribution with a mean value of 2.0 nm and an rms dispersion of 0.2 nm, in agreement with the assigned structure ($\text{TO}^+\text{Au}_{314}$, measuring 1.85 nm along the [111] and 2.25 nm along the [100] direction), assuming images arise from plane-projections of random nanocrystal orientations.

At the lowest beam intensities used, the images (facets) are quite stable; at moderate intensities, an evolution of the images attributable to nanocrystal rotations is frequently observed. Only at considerably higher electron fluxes do the particles transform in shape, accompanied by coalescence induced by loss of surfactant layer. Figure 2c illustrates the formation of locally ordered (2D superlattice) structures. A mean inter-particle (center-to-center) distance of 3.5 ± 0.2 nm has been determined from electron diffraction rings measured on this sample. It has been possible to obtain similar results, which are consistent with the measured masses and structural assignments (Table 1), for each highly purified fraction except the lightest.

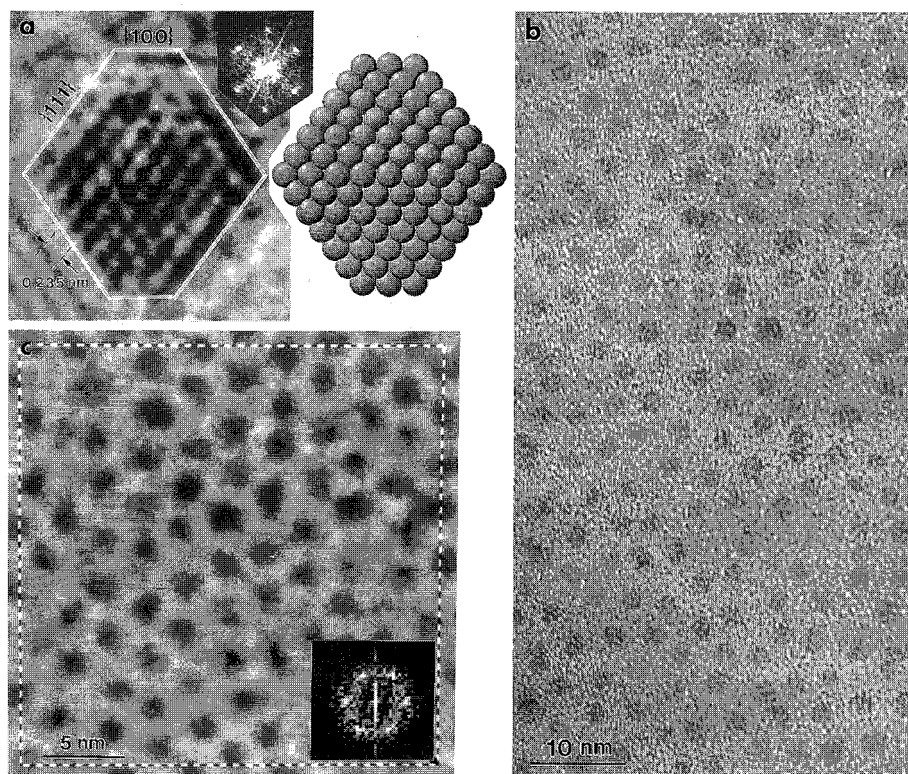


Fig. 2. Representative electron microscope (HREM) images of passivated gold nanocrystals in (sub)monolayer films from highly purified fractions spread on an amorphous carbon support. a) A high-resolution image of a single nanocrystal obtained from fraction I (see Table 1 and Fig. 1b), with its 2D-Fourier transform (inset), and a plane-projection of the theoretically predicted $\text{TO}^+\text{Au}_{459}$ structure. b) A large-area view containing some two hundred nanocrystals from fraction II. c) A single-domain area of locally ordered (2D-superlattice) structures selected from the area in (b), along with its 2D-Fourier transform.

Samples of these fractions condense reversibly to form molecular crystals, or 'nanocrystal superlattices', characterized by long-range translational and orientational order. Figure 3 shows a typical HREM image, the accompanying ED pattern, and a corresponding structural model, for an ultrathin (3-5 superlattice planes) multilayer film formed by condensation of fraction I (assigned $\text{TO}^+\text{Au}_{459}$, Fig. 1), exhibiting twinned superlattice monocrystalline domains. Similar long-range translational ordering has been demonstrated using low-dispersion (5 % by diameter) CdSe nanocrystal 2D arrays prepared by the Langmuir-Blodgett method, although without orientational ordering of the nanocrystals.^[10]

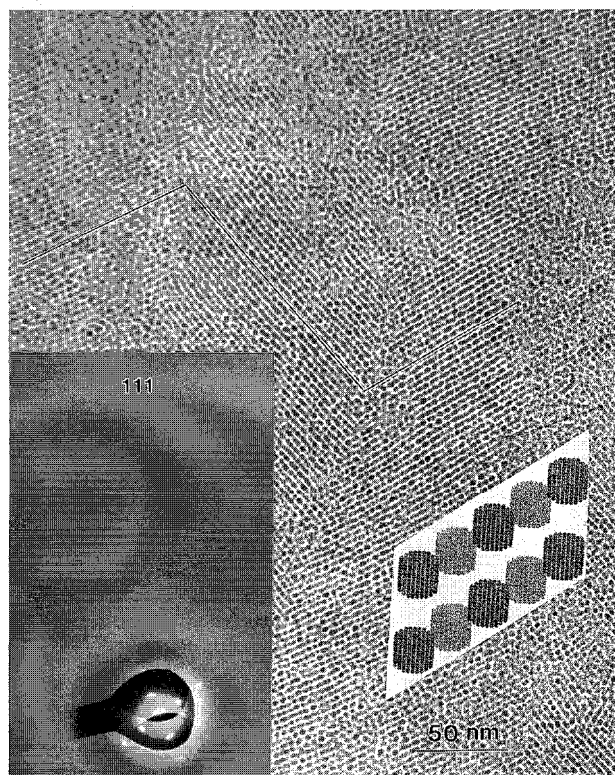


Fig. 3. An HREM image of an ultrathin crystalline film (nanocrystal superlattice) of fraction I, along with the corresponding electron diffraction (ED) pattern and a suggested structural model explaining these patterns and those obtained at higher resolution. See text for explanation.

The dominant observable features are rows of individual nanocrystals (each dark spot), with a projected inter-row spacing of 3.5 nm. Close analysis of this pattern, and comparison with X-ray diffraction information (Table 1), suggests that the image arises from a bcc superlattice viewed along a $[\bar{1}01]$ axis, as shown in the model (see inset). The individual nanocrystallites, $\text{TO}^+\text{Au}_{459}$ (see Figs. 1 and 2), are projected as dark (light) to indicate an upper (lower) position with respect to the viewer, and the surfactant monolayer is omitted for clarity. The model also shows a particular orientation (54.7°) of the $\text{TO}^+\text{Au}_{459}$ nanocrystals with respect to the $[010]$ rows of the superlattice, in which nine (111) gold planes (0.235 nm inter-plane spacing) are

evident, in agreement with images of the same film recorded at higher magnification. The diffraction pattern (inset at lower left) is a multiple-exposure photograph, and clearly shows two rings, each with four superlattice diffraction spots (two for each domain direction). The diffuse, outermost ring (labeled "111") corresponds to diffraction from the Au lattice planes within each nanocrystal.

Further structural information on separated fractions has been obtained by X-ray diffraction (XRD) measurements on polycrystalline films, typical examples of which are shown in Figure 4. The diffraction intensity appears in two distinct scattering regions—the small-angle (SA) and large-angle (LA) regions. The LA region shows broadened peaks (Fig. 4, right), whose shapes and intensities arise from diffraction from the finite number of atomic planes, indexed

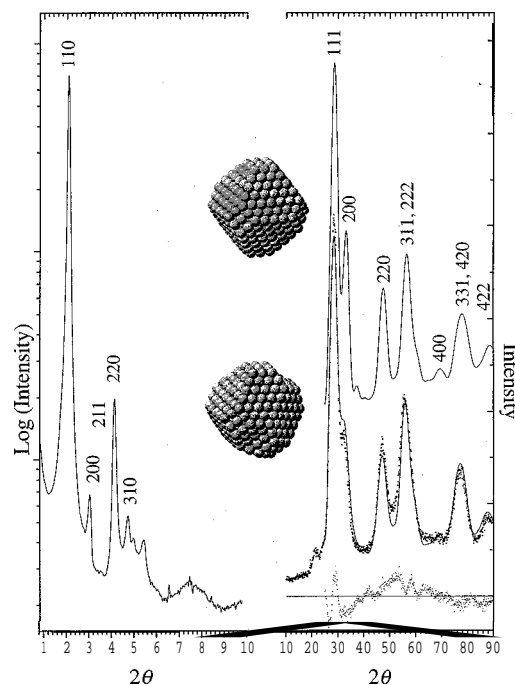


Fig. 4. Typical X-ray diffraction results (diffraction intensity vs. 2θ) for thick-film samples of fraction I, obtained using synchrotron radiation ($\lambda = 0.115$ nm X-rays) at near-grazing incidence (reflection mode). At left, the small-angle (SA) pattern ($10-90^\circ$) is plotted on a log. scale. At right, the large-angle (LA) pattern ($10-90^\circ$) is plotted on a linear scale as data points, and compared with powder-patterns calculated from the indicated structures (see text), along with the residual (dots below) for the better-fitting structure. The calculated pattern for the untwinned Au_{459} crystallite is shifted upward for clarity.

to fcc Au, in individual gold nanocrystallites. Powder X-ray patterns calculated for predicted structures of Au_{459} are also shown. The predicted pattern for singly-twinned crystallites is in good agreement with experiment. In these calculations, the faceted, relaxed TO^+ structure of Au_{459} and its nearly iso-energetic twinned variant are used, with no adjustable structural parameters, aside from 1 % uniform dilation of the fully relaxed structure.

Thermal damping is accounted for using a Debye-Waller factor with an effective Debye temperature of 220 K. This

“first-principles” mode of analysis should be contrasted with that prevalent in research on semiconductor nanocrystals,^[11] where multi-parameter fits employing generic spherical or spheroidal shapes are used, in the absence of specific, theoretically predicted, optimal structures,

The clear sequence of diffraction peaks in the SA region reveals the structure of the three-dimensional superlattice into which the fractionated samples of passivated nanocrystals crystallize (Fig. 3). By contrast, size-segregation in insufficiently isolated fractions is manifest by a multiplicity of (non-indexible) peaks in the SA-XRD patterns. Each sequence can be indexed, rather accurately, to a bcc superlattice. From the width of the first peak in such patterns, a lower bound on the grain size can be determined, ranging from 50 to 100 nm for the fractions considered here. Nanocrystal center-to-center nearest-neighbor distances D_{XRD} deduced from such analyses are given in Table 1. In each case, D_{XRD} is smaller than expected for the diameter of the passivated gold nanocrystal (the sum of the core diameter and twice the estimated surfactant layer thickness, ~ 1.5 nm, indicating that significant overlap of the passivating layers occurs in the condensed form.^[8]

These structural characterizations are significant steps toward the ultimate demonstration of distinct, new, molecular materials, involving resolution of their structures through single-crystal X-ray diffraction. This is a task that, for molecular volumes approaching 100 nm^3 , is comparable to determining the crystal structure of a large globular protein, and has rarely been achieved for materials composed of inorganic nanocrystals (inorganic macromolecules), including compounds (a $(\text{Cu}_2\text{Se})_{65}$ nanocrystal, with ligands, being the largest^[12]), binary semiconductors,^[13] and mixed metals.^[14] Structure determination of elemental nanocrystals by single-crystal XRD remains an outstanding challenge. Nonetheless, progress toward this goal has been achieved, as indicated by the highly diffractive thin films and also by the growth of small single crystals. An example of the latter is illustrated by Figure 5, which shows a well-faceted crystal grown from fraction I (assigned to Au_{459}).

A range of bonding, electronic, optical, thermal, chemical, and materials properties have been investigated on mixed and purified forms of these passivated gold nanocrystals. Only a brief listing of the properties of the systems is possible here:^[15]

- Spectroscopic evidence confirms that the bonding and electronic structure characteristics are fully analogous to those of extended-surface Au-SR SAMs.^[2,16]
- The characteristic optical absorption band, associated with the bright color of colloidal Au,^[17] is modified systematically with descending nanocrystal size, with discrete (quantum level) features evident for the smallest two fractions; optically flat dry films appear bronze-to-gold (see also crystals in Fig. 5).
- They are stable in dilute solution to 160°C , above which the surfactant layer desorbs rapidly,^[18] and to at least 250°C in solution with excess thiol.

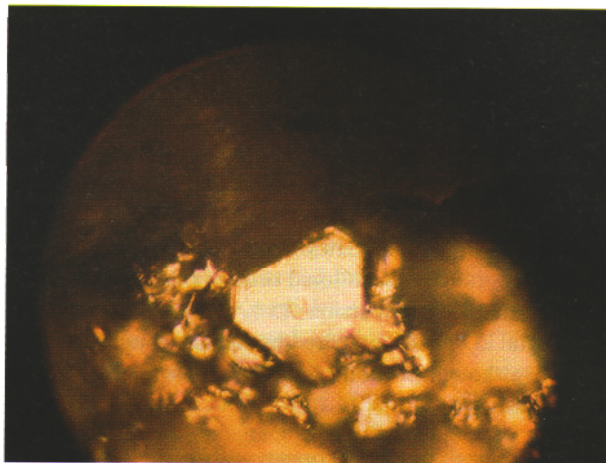


Fig 5 Optical micrograph of crystals grown from the highly purified fraction I. The large crystal at center measures $\approx 40 \mu\text{m}$ in length

- Solutions and films exposed to intense laser radiation are stable (completely redispersible) up to the ablation threshold.
- They are generally inert, even when exposed to strong acid or base, but undergo thermally-assisted quantitative exchange reactions^[19] in solution with the same (auto-)exchange) or different thiols of various chain-length or terminal group, leading to systematic modification of materials form and properties.
- They are highly soluble in nonpolar solvents (approaching $40 \text{ mg}/\text{cm}^3$), soluble in slightly polar solvents, and completely insoluble in short-chain alcohols or water, reflecting a high surface hydrophobicity revealed also by contact angles exceeding 90° for water droplets on optically flat films.
- They are also characterized by very low friction (lateral) forces measured by scanning force microscopy. These microscopic and materials properties are consistent with a structural model^[8] in which sulfur head groups form a compact, ordered layer passivating the underlying faceted gold nanocrystallite, and the hydrocarbon chains offer a compact protective coating whose structural nature depends on chain-length, temperature, and its environment (e.g., isolated, solution-phase, or condensed into the solid state).

In summary, through the use of surfactants (self-assembled monolayers) that are capable of etching imperfect structures and of passivating crystal facets in a compact manner compatible with the underlying crystallite surface structure, one is led to highly stable and versatile molecular nanocrystal materials. These passivated elemental (gold) nanocrystals are of a molecular nature, retaining their integrity in solution, as solids or thin films where they exhibit crystalline (translational and orientational) order, and in the (transient) gas phase as established by the success of laser-desorption mass spectrometric analysis. Underlying the self-selecting abundance pattern of these materials is a

discrete sequence of energetically optimal fcc structures of a truncated octahedral morphological motif. Evidence for the formation of such a discrete sequence of nanocrystal gold molecules, rather than the appearance of a continuous distribution of sizes and structures, has been established and confirmed through independent measurements, including: size-segregation in precipitation of mixed samples; mass spectrometric detection capable of resolving even small (less than 10 %) quantities of species differing in size by less than one lattice spacing; invariance of the sequence and observed properties to the details of the preparation and separation procedures; and structural analyses performed on isolated fractions of the sequence, guided by, and correlated with, theoretical predictions. The discrete nature and stability of such nanocrystal materials and the size-evolutionary patterns of their properties, including their propensity to form extended superlattices, suggest ways and means for the design and fabrication of advanced optical, electronic, (photo)-catalytic and sensor materials of controlled characteristics.

Experimental

The separations are performed, starting from nearly-saturated toluene solutions of nanocrystal mixtures (typically 10 mL of 20 mg/mL concentration), and slowly adding a miscible non-solvent (usually acetone) by passive vapor transfer, until the solution volume is increased by a predetermined amount [21]. The solution is then isolated, allowed an extended equilibration period while stirring, and then centrifuged and decanted to remove the soluble fraction from the precipitated fraction, each of which is analyzed by MS. The procedure is then repeated separately on both fractions, and so on, to generate many further fractions, until a handful of highly purified fractions are obtained which are incapable of further separation and which show single clear onsets in the mass spectra. All such fractions are obtained from several distinct batches and are independent of the precise procedure followed. This separation process invariably precipitates fractions in order of descending nanocrystal mass.

The mass spectra are obtained by the laser-desorption/ionization and time-of-flight (TOF) methods, using a custom-built 1.2 m instrument. Neat or matrix-diluted films are prepared on steel rod tips by vacuum-drying of toluene solutions of passivated nanocrystals. The rods are inserted into the ion-source region of the TOF mass spectrometer, and are irradiated by the unfocused output of a frequency-doubled Nd:YAG laser (532 nm 5 ns) at a pulse fluence of 20 mJ/cm². The mass spectra shown are for negatively charged particles (similar results of reduced signal-to-noise are observed at other wavelengths and for positive-ion mode), in which case a 15 kV initial acceleration and a 30 kV post-flight acceleration is provided prior to impact on a conversion-type detector. Digitized TOF waveforms are averaged, calibrated against those of biomolecules in the 10–60k range and corrected for desorption ejection velocity, and converted to a mass-scale. Calibration in the pulsed-voltage mode is considerably less accurate because of complexities inherent in the method of [22]. The spectrum shown in the Figure 1e inset has been obtained on the custom high-resolution time-of-flight instrument at the Max-Planck-Institut für Festkörperforschung in Stuttgart, using a similar desorption arrangement to that mentioned above, but displaced 10 cm from the collection volume. Positive ions are extracted at right angles into the ca. 4-m reflectron, and spectra are recorded in ion-counting mode.

For HREM measurements (Figs. 2 and 3), monolayer-coverage samples are prepared by spreading toluene solutions, of precisely determined concentrations, on amorphous carbon substrates, and subsequently allowing the fluid film to slowly dry in a small covered container. Multilayer films are prepared similarly by reversible condensation from more concentrated solution onto an amorphous-carbon support. The images were recorded on a cold field-emission Hitachi HF-2000 instrument (200 keV beam energy), at magnifications of 500 k (Fig. 2a), 700k (b), and 60k (c). The high coherence of the electron beam produces interference (Fresnel) fringes, for example in the lower left of frame 2a.

Thick films are prepared for XRD measurements on flat crystalline substrates, usually Si wafers, by evaporation of highly concentrated solutions

followed by extended drying. Larger crystals, of the size shown in Figure 5, are grown by a procedure similar to that used for separating mixtures, except that the precipitation takes place over a period of several days from a slowly stirred toluene-acetone solution of a highly purified fraction. Precipitated crystals are washed repeatedly with acetone, and then allowed to dry under ambient conditions.

Added Note: Since the time that the work reported herein had been substantially completed (1 June 1995), several reports have appeared concerning either thiol-passivated gold nanocrystals or nanocrystal superlattices of other materials. Dorogi et al. [23] and Brust et al. [24] have prepared gold nanocrystals passivated by SAMs in which the organic surfactant contains thiol groups at both ends, permitting the assemblies to be chemically bound to each other [24] or to a gold-film [23]; both reports focus on electrical transport properties, the first on single-assembly conductance and the latter on transport in three-dimensional arrays. Ohara et al. [25] reported on the formation and local structure of small collections of mixtures of gold nanocrystals passivated by alkylthiolate surfactant. Terrill et al. [26] have also prepared and measured aggregate properties of SAM-passivated gold nanocrystals. Murray et al. [27] reported the formation and structure of nanocrystal superlattices comprised of passivated CdSe nanocrystals; the quantitative contents of that report are XRD results indicating superlattice ordering (crystal quality) that is similar, but consistently inferior, to that shown here (in Fig. 4 and Table 1) and first reported contemporaneously [28].

Received: January 3 1, 1996

- [1] R. P. Andres et al., *J. Mater. Res.* **1989**, 4, 704.
- [2] R. G. Nuzzo, D. L. Allara, *J. Am. Chem. Soc.* **1983**, **105**, 481.
- [3] M. M. Alvarez, unpublished.
- [4] M. Brust, M. Walker, D. Bethell, D. J. Schiffrin, R. Whyman, *J. Chem. Soc. Chem. Commun.* 1994, 801
- [5] K. Edinger, A. Gölzauer, K. Demota, C. Wöll, M. Grunze, *Langmuir* **1993**, 9, 4.
- [6] H. Weller, *Adv. Mater.* **1995**, 7, 94.
- [7] a) C. L. Cleveland, U. Landman, *J. Chem. Phys.* 1991, 94, 7376. b) C. L. Cleveland et al., unpublished.
- [8] W. D. Luedtke et al., unpublished.
- [9] J. B. Adams, S. M. Foiles, W. G. Wolfer, *J. Mater. Res.* **1989**, 4, 102.
- [10] B. O. Dabbousi, C. B. Murray, M. F. Rubner, M. G. Bawendi, *Chem. Mater.* **1994**, 6, 216.
- [11] C. B. Murray, D. J. Norris, M. G. Bawendi, *J. Am. Chem. Soc.* 1993, 106, 6285.
- [12] H. Krautscheid, D. Fenske, G. Baum, M. Semmelman, *Angew. Chem. Int. Ed. Engl.* **1993**, 32, 1303.
- [13] N. Herron, J. C. Calabrese, W. E. Farneth, Y. Wang, *Science* **1994**, 259, 1426.
- [14] A. Cierotti, F. Demartin, G. Longoni, M. Manassero, M. Marchionna, G. Piva, M. Sansoni, *Angew. Chem. Int. Ed. Engl.* **1985**, 24, 697. For a review, see G. Schmid, *Chem. Rev.* 1992, 92, 1709.
- [15] J. T. Khoury et al., unpublished.
- [16] C. D. Bain, E. B. Troughton, Y.-T. Tao, J. Evall, G. M. Whitesides, R. G. Nuzzo, *J. Am. Chem. Soc.* **1989**, **111**, 321.
- [17] M. Faraday, *Phil. Trans. R. Soc. London* 1857, 147, 145.
- [18] R. G. Nuzzo, B. R. Zegarski, L. H. Dubois, *J. Am. Chem. Soc.* **1987**, **109**, 733.
- [19] H. Biebuyck, C. D. Bain, G. M. Whitesides, *Langmuir* **1994**, 10, 1825.
- [20] S. Murthy et al., unpublished.
- [21] A. Chemseddine, H. Weller, *Ber. Bunsenges. Phys. Chem.* 1993, 97, 636.
- [22] G. R. Kinsel, M. V. Johnston, *Int. J. Mass Spec.* **1989**, 91, 157.
- [23] M. Dorogi, J. Gomez, R. Osifchin, R. P. Andres, R. Reifengerber, *Phys. Rev. B* **1995**, 52, 9071.
- [24] M. Brust, D. Bethell, D. J. Schiffrin, C. J. Kiely, *Adv. Mater.* **1995**, 7, 795.
- [25] P. C. Ohara, D. V. Leff, J. R. Heath, W. M. Gelbart, *Phys. Rev. Lett.* **1995**, 75, 3466.
- [26] R. H. Terrill et al., *J. Am. Chem. Soc.* 1995, 117, 12537.
- [27] C. B. Murray, C. R. Kagan, M. G. Bawendi, *Science* **1995**, **270**, 1335.
- [28] Earlier reports on this work have been presented at the ISSPIC-7 Conference in Kobe, Japan, September 1994, and at a NATO-ASI Workshop, Erice, Italy, June 1995, and are in press: "Nanocrystal Gold Molecules (R. L. Whetten, J. T. Khoury, M. M. Alvarez, Srihari Murthy, I. Vezmar, Z. L. Wang, C. L. Cleveland, W. D. Luedtke, U. Landman) in *Proc. June 1995 Conf. Chemical Physics Of Fullerenes 5 and 10 Years Later*" in Varenna, Italy; (Ed: Andreoni) Kluwer, Dordrecht **1996**.